

## Nontrivial metallic state of MoS<sub>2</sub>

Zi-Yu Cao,<sup>1,2,3</sup> Jia-Wei Hu,<sup>3</sup> Alexander F. Goncharov,<sup>1,4</sup> and Xiao-Jia Chen<sup>1,3,\*</sup>

<sup>1</sup>Key Laboratory of Materials Physics, Institute of Solid State Physics, Chinese Academy of Sciences, Hefei 230031, China

<sup>2</sup>University of Science and Technology of China, Hefei 230026, China

<sup>3</sup>Center for High Pressure Science and Technology Advanced Research, Shanghai 201203, China

<sup>4</sup>Geophysical Laboratory, Carnegie Institution of Washington, Washington, DC 20015, USA



(Received 21 January 2018; revised manuscript received 7 June 2018; published 22 June 2018)

The electrical conductivity and Raman spectroscopy measurements have been performed on MoS<sub>2</sub> at high pressures up to 80 GPa and variable temperatures down to 5 K. We find that the temperature dependence of the resistance in a mixed phase has an anomaly (a hump) which shifts with pressure to higher temperature. Concomitantly, a different Raman phonon mode appears in the mixed state suggesting that the electrical resistance anomaly may be related to a structural transformation. We suggest that this anomalous behavior is due to a charge-density wave state, the presence of which is indicative for an emergence of superconductivity at higher pressures.

DOI: [10.1103/PhysRevB.97.214519](https://doi.org/10.1103/PhysRevB.97.214519)

### I. INTRODUCTION

Two-dimensional (2D) materials are characterized by a strong anisotropy of the intra- versus interlayer bonding. This remarkable difference brings up unique notions such as 2D materials which can be exploited for practical applications [1]. One of the most exposed materials of such a kind is graphene [1,2], which also brought the interest to inorganic materials with unique electronic [3], optical [4] attributes and high mobility [5]. However, graphene is a gapless (semimetallic) material which restricts its possible applications. In contrast, the transition-metal dichalcogenides (TMDs), quasi-2D material with distinct structures, and unique physical properties [6–10] possess a nonzero band gap that could also be tuned. Therefore, TMDs are currently attracting enormous research interest. MoS<sub>2</sub> is one of the most extensively investigated member of TMDs, and it can be prepared as a 2D material via mechanical exfoliation [4,11]. By varying the number of layers, MoS<sub>2</sub> can be transformed from an indirect band-gap semiconductor to a direct band-gap semiconductor [11]. Monolayer MoS<sub>2</sub> has mechanical properties almost as good as graphene, but unlike graphene, it possesses a direct band gap. Thus, MoS<sub>2</sub> shows an excellent potential to replace graphene in the next generation nanoelectronics applications [12–16]. Monolayer MoS<sub>2</sub> is predicted to form charge-density wave (CDW) state [17]. In addition, by heavily hole doping monolayer MoS<sub>2</sub> transforms from a semiconductor to a metallic state and eventually enters a superconducting state [18,19]. Similar structural effects related to *2H* to *1T* transition (from trigonal to octahedral TM coordination) have been found in other doped TMDs (MoTe<sub>2</sub>), confirmed by Raman spectroscopy measurements [20] including the case when the *1T* phase has been stabilized by pressure and superconductivity appears accordingly [21].

The application of external pressure is an alternative (to doping) way to tune the electronic as well as crystal structure. MoS<sub>2</sub> transforms from a *2H<sub>c</sub>* to a *2H<sub>a</sub>* phase (through a sliding of the layers) above 20 GPa along with a metallization [22,23]. However, the resistivity measurements show that the temperature dependence of the resistivity is not monotonous revealing a pressure-dependent hump in the resistivity-temperature curves [22]. This suggests an additional electronic or structural ordering in MoS<sub>2</sub> at low temperatures and high pressures. It is common for TMDs with both major structural types *2H* and *1T* to demonstrate CDW phenomena, which lower the symmetry of their quasi-2D structures [24–28]. It has been noticed that the presence of CDW indicates the proximity of a superconducting state emerging at lower temperatures. These two states have been shown to demonstrate the competing orders which could also be applied to high-temperature superconductors [29]. The highest superconducting critical temperature ( $T_c$ ) is observed in materials with CDW ordering that occurs at the comparable temperatures [30,31]. Superconductivity in MoS<sub>2</sub> has been observed at high pressures above 90 GPa [32] and for heavily doped 2D materials [18]. However, the nature of superconductivity remains unclear.

In this work, we report on the electrical transport and Raman spectroscopy measurements of MoS<sub>2</sub> at high pressures and low temperatures. Anomalies are discovered in both the resistance-temperature (R-T) curves and the Raman spectra. A hump in the R-T dependence has been observed increasing in temperature with pressure. In the mixed phase a Raman band appears increasing in intensity with pressure and then diminishing on cooling down. We connect the R-T hump and this Raman feature as well as an anomalous behavior of the regular phonon modes with developing a CDW order on MoS<sub>2</sub> at high pressure by analogy with observations of similar states in other (commonly heavier) TMDs. Furthermore, this order is indicative for the competition with superconductivity at higher pressures.

\*xjchen@hpstar.ac.cn

## II. EXPERIMENTAL DETAILS

Four MoS<sub>2</sub> samples have been investigated in separate electrical resistance (A) and Raman (B, C, and D) experiments. For electrical resistance (A) measurements, a miniature diamond-anvil cell with anvils in a 300- $\mu\text{m}$  culet was used. A sample chamber of diameter 120  $\mu\text{m}$  was formed by drilling in the *c*-BN gasket positioned then situated between tips of two diamond anvils. Four Pt wires were adhered to the sample with silver epoxy by the Van Der Pauw method [33] to measure the in-plane resistance. Daphne oil 7373 was used as a pressure transmitting medium to ensure hydrostatic pressure conditions in the sample chamber. The pressure was determined by the spectral shift of the ruby fluorescence R1 peak. Resistance was measured in a physical property measurement system (by Quantum Design). For Raman (B, C, and D) experiments, a Mao-Bell diamond-anvil cell with a 200- $\mu\text{m}$  culet, low fluorescence diamonds, and rhenium gasket combined with a He continuous flow cryostat was used for high-pressure and low-temperature Raman measurements. Neon was loaded as the pressure transmitting medium. Pressure was measured *in situ* at high pressure and low temperatures using a ruby fluorescence technique. The temperature was measured using Pt resistance sensors attached to the diamond-anvil cell close to the sample with a typical precision of  $\pm 0.5$  K. The Raman spectra were measured using a single stage spectrograph equipped with an array thermoelectrically cooled charge-coupled device detector. The Raman notch filters were of a very narrow bandpass (Optigrate) allowing Raman measurements down to 10  $\text{cm}^{-1}$  in Stokes and anti-Stokes [34]. The 488-nm excitation line was used to illuminate an approximately  $5 \mu\text{m} \times 5 \mu\text{m}$  spot on the newly cleaved shining surface of MoS<sub>2</sub>. The Raman spectra were measured with laser power down to 1 mW to avoid laser heating effects. The heating effects are quantified by the ratio of the anti-Stokes to Stokes Raman intensity [35] at room temperature and found to be 3–12 K.

## III. RESULTS AND DISCUSSION

Figures 1(a) and 1(b) display the R-T curves obtained at various pressures around the semiconductor-metal transition. The resistance declines by 3 magnitude with increasing pressure up to 27.3 GPa at room temperature. Below 20 GPa, the R-T curves exhibit an overall semiconducting behavior, but a hump is observed reversing the slope in the temperature interval below the maximum. When pressure is increased above 20 GPa, a phase transition from  $2H_c$  to  $2H_a$  occurs [22,23], and the system turns into a mixed state [36,37]. However, we find that above 20 GPa, the R-T curves show an anomaly, where a generally metallic behavior turns into a semiconducting one at temperatures above the hump. Moreover, the R-T slope is nearly zero (if not negative) in the limit of low temperatures. The hump is moving to higher temperatures with pressure.

The presence of a hump in the R-T curve is a common behavior for TMDs and it was related to the presence of CDW state [38], which results in a crossover on the resistance behavior due to the electronic scattering by CDW fluctuation changing the R-T slope and character at low temperatures. This behavior can also be considered as due to the fact that a portion of the Fermi surface becomes gapped in the CDW state [39].

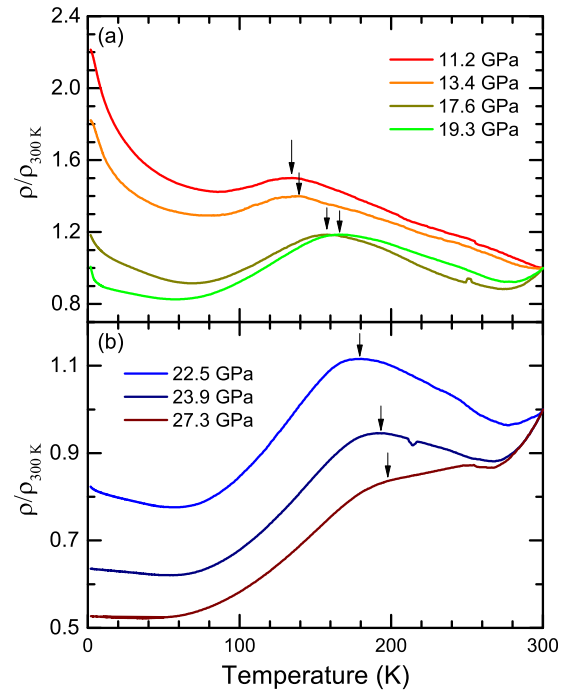


FIG. 1. Temperature dependence of the resistance of MoS<sub>2</sub> at various pressures measured at 300 K. (a) Semiconducting behavior at pressures below 20 GPa. (b) Metal behavior at pressures between 20 and 30 GPa. The arrows indicate the lock-in temperatures at various pressures.

Meanwhile, the CDW gap also leads to a sign reversal in the Hall coefficient [38] and a promotion of magnetoresistance. As a quasi-2D compound, MoS<sub>2</sub> has immense potential to enter into the CDW state below a certain temperature. Thus, the CDW state is a possible candidate in the observed nontrivial metallic state (Fig. 1).

For better understanding of the nontrivial metallic state, we performed Raman measurements in the pressure-temperature range of interest near the  $2H_c$  to  $2H_a$  transition and in high-pressure phase up to 80 GPa (Figs. 2–5). The  $2H_c$  to  $2H_a$  transition is isostructural, so the same Raman fundamental modes are expected to be observed in the spectra:  $A_{1g} + E_{1g} + 2E_{2g}$ . At ambient conditions these modes are observed at 32 ( $E_{2g}^2$ ), 287 ( $E_{1g}$ ), 381 ( $E_{2g}^1$ ), and 409 ( $A_{1g}$ )  $\text{cm}^{-1}$  [40]. Our low-temperature Raman spectra demonstrate that these modes behave quite similarly to the observations reported at room temperature [22]. However, the  $E_{1g}$  and  $E_{2g}^2$  modes are weak (see also Refs. [24,27] for other TMDs), and could not be observed in some of our spectra. In addition, in some Raman experiments (e.g., sample B) we have observed Raman-forbidden modes above the position of the  $A_{1g}$  mode, which we tentatively assigned to out-of-plane  $A_{2u}$  and  $B_{2g}$  infrared and inactive modes [42], respectively. As in Ref. [22], we find that  $E_{2g}^2$  and  $E_{2g}^1$  modes show discontinuities in frequency, while the  $A_{1g}$  mode changes the pressure slope demonstrating the  $2H_c$  to  $2H_a$  transition. At 5.7 K the transition starts at 25 GPa and is completed at nearly 50 GPa compared to the 20–40-GPa range at room temperature [22]. Based on the results of previous experiments [22], our temperature runs at 20.9, 34.8, and 47.6 GPa (Fig. 2) should be referred to

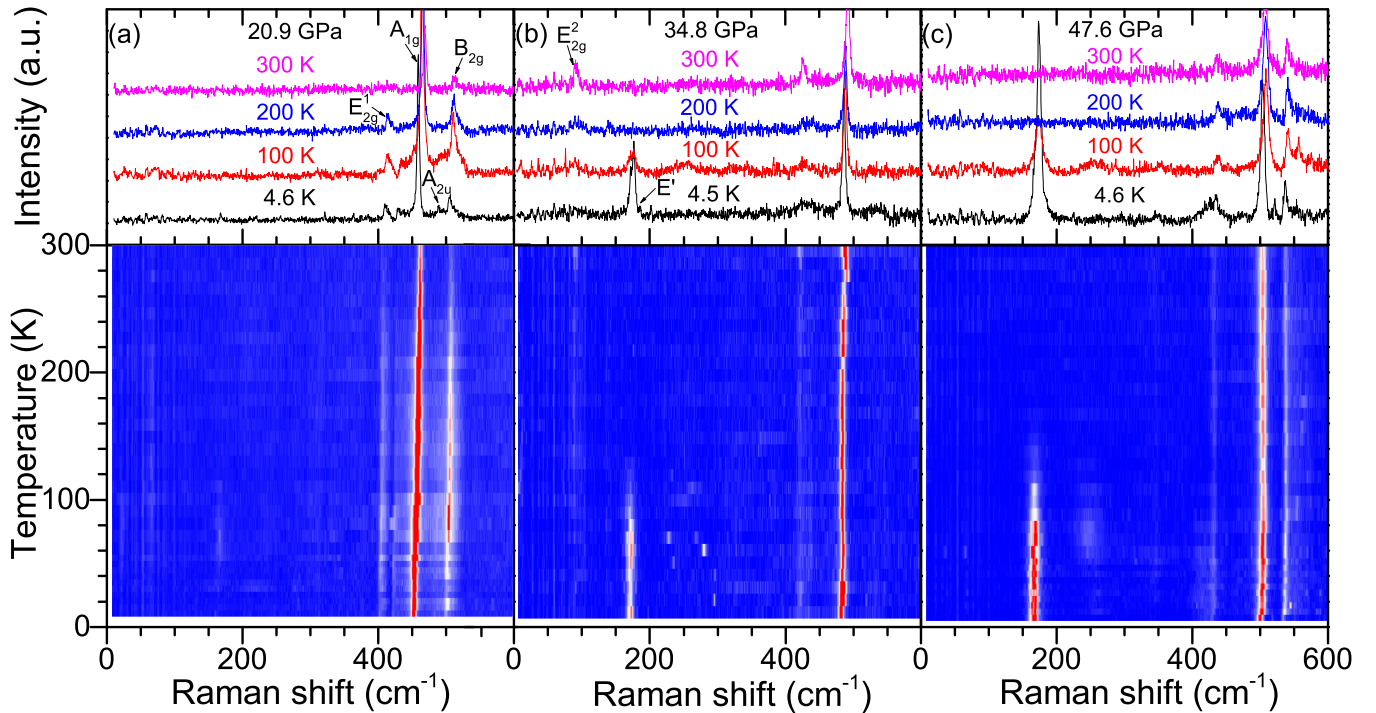


FIG. 2. Raman data of MoS<sub>2</sub> at various temperatures at 20.9 GPa (sample B) (a), 34.8 GPa (sample C) (b), and 47.6 GPa (sample B) (c). The upper panels are the spectra at various temperatures and the bottom panel is the 2D presentation in the Raman frequency-temperature coordinates.

semiconducting  $2H_c$ , mixed  $2H_c$  and  $2H_a$ , and mainly metallic  $2H_a$  phases, respectively.

A different mode at  $174\text{ cm}^{-1}$  ( $E'$ ) appears in the  $2H_c + 2H_a$  mixed phase at 34.8 GPa [Fig. 2(b)] at low temperature. This mode becomes very strong at 47.6 GPa [Fig. 2(c)]. In the temperature scans at 34.8 and 47.6 GPa, the intensity of this  $E'$  mode stays almost constant below approximately 60 K,

and then drops down. The mode nearly vanishes above 140–170 K (Fig. 3). The frequency of the  $E'$  mode remains essentially unchanged. At 47.6 GPa, the  $2H_c$  phase shows an extremely weak response from the Raman spectra. However the intensity of the  $E'$  mode gets much stronger. Compared with 34.8 GPa, only the ratio of the  $2H_a$  phase in mixed phases is increased. The  $E'$  mode is thus generated in the  $2H_a$  phase. The origin of this  $E'$  peak is likely a phonon mode as will be discussed below. Concomitantly, other phonon modes show anomalous temperature dependencies. Figure 3 displays the details of the temperature dependence of the normalized intensity of the  $E'$  mode and the frequency of the  $A_{1g}$  mode at 34.8 and 47.6 GPa, respectively. The temperature dependence of the frequency of the  $A_{1g}$  mode changes the slope at the lock-in temperature and exhibits a softening behavior above 150 K. The softening behavior might be caused by the competition between the  $2H_a$  and the  $2H_c$  phases as well as the impact of the  $E'$  mode. As the pressure is increased up to 47.6 GPa, the  $2H_a$  phase is the dominance in MoS<sub>2</sub> [22,23]. The  $A_{1g}$  mode first hardens above 160 K, and then softens below 160 K. The anomalous temperature in the  $A_{1g}$  mode accords with the appearance of the  $E'$  mode as well. These anomalous changes suggest the presence of an additional phase transition or electronic ordering, which we tentatively assign to CDW.

The CDW state is a common nature in TMDs. In Raman spectra, TMDs with CDW order constantly contain a soft multiphonon mode [41]. However, this is missing here. It is verified that the frequency of the multiphonon mode is related to the soft phonon around the CDW wave vector in phonon dispersion spectra (Kohn anomaly). However, the soft phonon is far away from the  $\Gamma$  points. The soft phonon

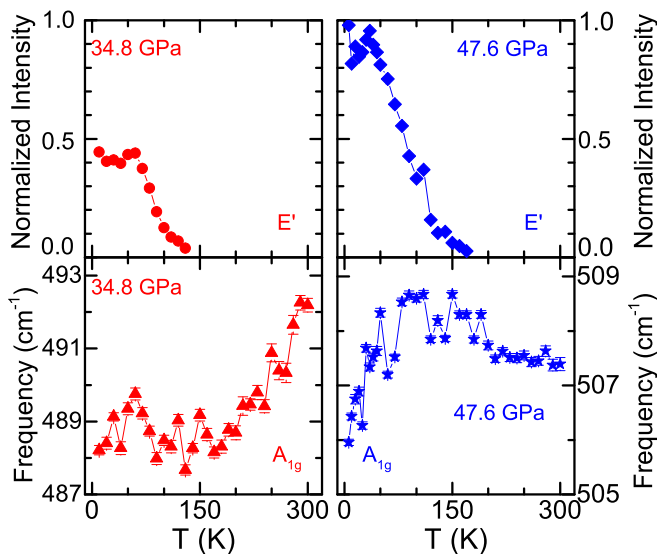


FIG. 3. The temperature dependence of the normalized intensity of  $E'$  mode (upper panels) and the frequency of  $A_{1g}$  mode (lower panels) at 34.8 (red) and 47.6 GPa (blue). The  $E'$  mode is normalized by the intensity of  $E'$  mode at 4.6 K and 47.6 GPa.

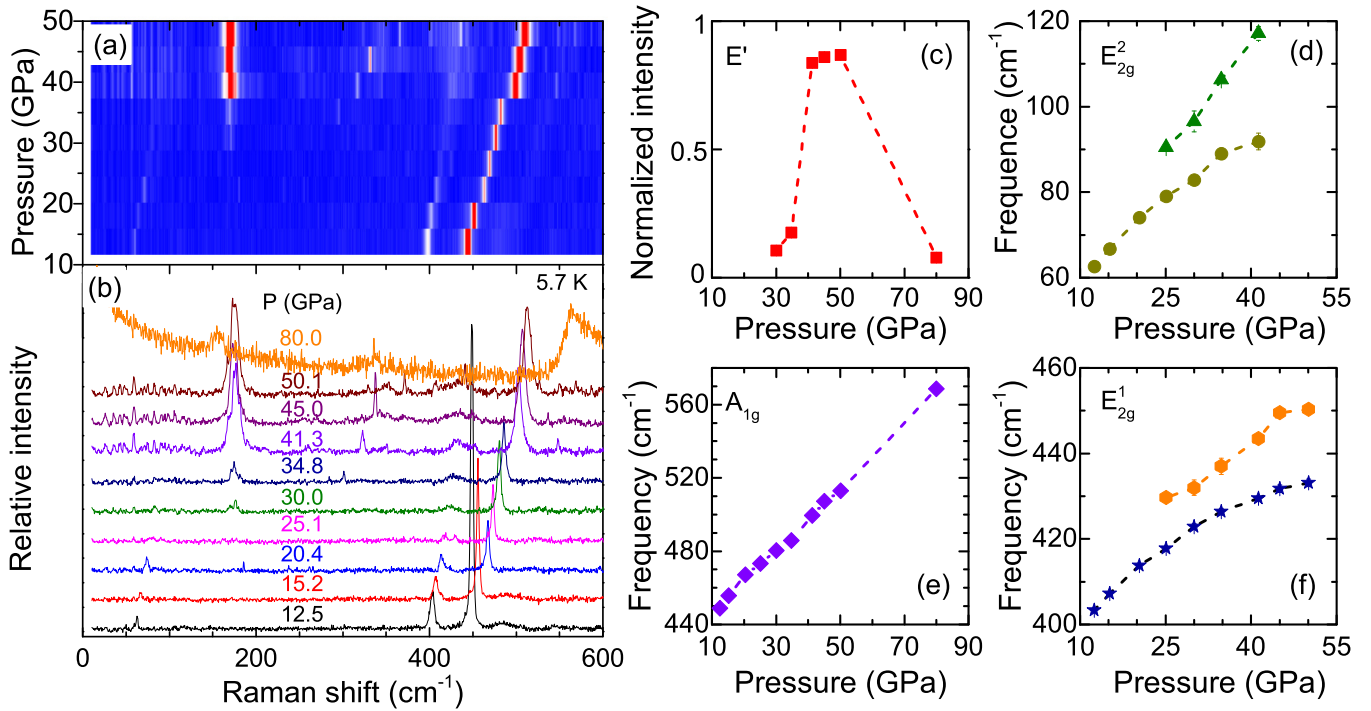


FIG. 4. Raman data of MoS<sub>2</sub> at temperature of 5.7 K and various pressures up to 80.0 GPa. (a) The 2D map of the Raman intensity at 5.7 K in the frequency-temperature coordinates. (b) Raman spectra at various pressures at 5.7 K. (c) The pressure dependence of the intensity of the  $E'$  mode at 5.7 K. The pressure dependence of the Raman frequencies of the  $E_{2g}^2$  (d),  $A_{1g}$  (e), and  $E_{2g}^1$  (f) modes at 5.7 K.

in phonon dispersion spectra shouldn't have a direct Raman active. In Raman spectra, the soft multiphonon mode originates from the anharmonicity. Therefore, the missing of the soft mode in Raman spectra is mainly because of the weak anharmonicity. The  $E'$  mode likely roots in CDW order. However it doesn't belong to the CDW amplitude mode since it is insensitive with temperature. The  $E'$  mode is in a good correspondence in frequency with a transverse acoustic mode near the Brillouin-zone boundaries at the  $K$  and  $M$  points [42,43]. The position of this mode at ambient pressure is near 170  $\text{cm}^{-1}$ . However, it is difficult to judge about the position of the zone-boundary acoustic modes because their pressure dependence is unknown in the semiconducting  $2H_c$  phase and there may be a discontinuity at the layer sliding  $2H_c + 2H_a$  transition, assuming that the  $E'$  mode has the phonon origin and given its weak temperature dependence. One can propose that the appearance of this mode in the Raman spectra manifests the development of a superstructure, which results in the Brillouin-zone folding [25]. Apart from an obvious possibility of a structural phase transition, CDW has been shown to produce periodic lattice distortion leading to observations of nominally forbidden Raman bands.

Furthermore, the Raman spectra at a fixed temperature of 5.7 K through the *in situ* change of pressures were collected with sample D. Figures 4(a) and 4(b) clearly depict all changes in every single mode. Figures 4(d)–4(f) illustrate the pressure dependence of the frequencies of the Raman-active modes  $E_{2g}^2$ ,  $A_{1g}$ , and  $E_{2g}^1$ , respectively. All these phonon modes gradually harden. However, around 25 GPa, the frequency of the  $A_{1g}$  mode changes the slope. More special features are observed in the  $E_{2g}^2$  and  $E_{2g}^1$  modes. Both the  $E_{2g}^2$  mode and the  $E_{2g}^1$

mode divide into two modes at 25 GPa. At room temperature, the same feature indicates the phase transition from the  $2H_c$  to  $2H_a$  [22]. At 5.7 K, the split of these modes continues up to 50.1 GPa. This indicates that MoS<sub>2</sub> enters a mixed state. However, in the electrical conductivity measurements the mixed state

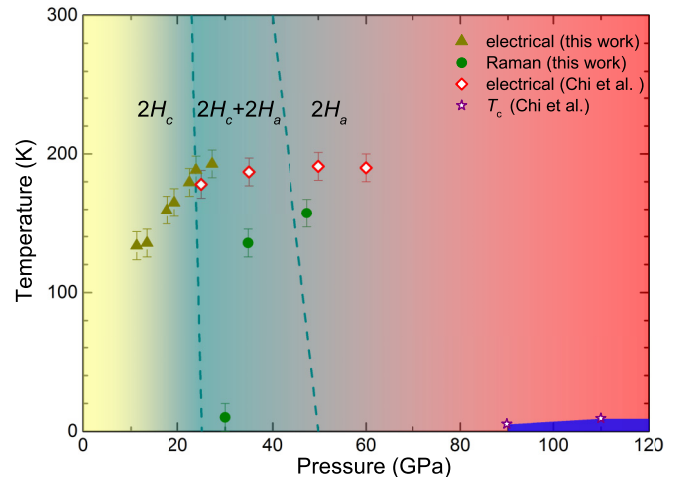


FIG. 5. Phase diagram illustrating the results. The dark cyan dot-dashed lines are the phase lines (separating pure  $2H_c$ , mixed, and  $2H_a$  phases determined from Raman spectroscopy in this work at 5.7 K and Ref. [22] at 297 K). The lock-in temperatures of this work are the filled symbols (dark yellow triangle from resistance and green square from Raman spectra). The results from the works of Chi *et al.* [22,32] by electrical transport measurement are open symbols (red diamond indicated the anomalous temperature and purple star for  $T_c$ ).

behaves like a metal if the composition of the  $2H_a$  phase is above the percolation limit. Above 25 GPa, an additional  $E'$  mode, located around  $174\text{ cm}^{-1}$ , appears at 5.7 K, and the  $E'$  mode exists in the entire pressure range between 25 and 80 GPa. However, this phonon mode is absent at 5.7 K below 25 GPa. Therefore, the presence of the  $E'$  mode is a unique feature exhibited in the  $2H_a$  phase. Although the  $E_{2g}^2$  mode and  $E_{2g}^1$  mode split above 25 GPa, the phonon modes in the  $2H_a$  phase stiffen regularly with increasing pressure. The pressure dependence of the intensity of the  $E'$  mode is shown in Fig. 4(c). The intensity of the  $E'$  mode first increases upon compression until 50.1 GPa. However, although  $E'$  is the pressure induced mode, the energy and the intensity of the  $E'$  mode is reduced at certain pressure. At 80 GPa, just below the pressure where the superconductivity sets in at low temperature at 90 GPa [32], the  $E'$  mode, with significant decrease in the intensity, shifts from  $174$  to  $156\text{ cm}^{-1}$ .

The phase diagram of MoS<sub>2</sub> is mapped out by combining the Raman-scattering and resistance data [22,32]. At room temperature and high pressures, the  $2H_c$ -MoS<sub>2</sub> has been shown to change the structure that is due to the layer sliding, formation of the  $2H_c + 2H_a$  mixed phase at 23 GPa, and eventually the  $2H_a$  phase at 40 GPa. The Raman spectra at high pressures and low temperatures revealed that the mixed phase starts from 25 GPa and survives to higher pressure up to 50 GPa. We therefore divided the phase diagram into three parts which represent the  $2H_c$ ,  $2H_c + 2H_a$ , and  $2H_a$  phase. The hump in resistance and the lock-in temperature of the  $E'$  mode are also plotted in Fig. 4. The lock-in temperature related to this phonon anomaly is comparable to that where the hump in electrical resistance appears at pressures above 50 GPa, but disagrees at lower pressures. This is likely because the phonon anomalies can only be observed in the  $2H_a$  phase states (including mixed  $2H_c + 2H_a$ ), while the conductivity hump could be observed in the  $2H_c$  semiconducting and  $2H_c + 2H_a$  mixed phase samples.

Theoretical researches have discussed the possibility of CDW in MoS<sub>2</sub> [17], but in relations to another underlying crystal structure,  $1T$ , which makes the results not immediately applicable to the high-pressure  $2H_a$  polymorph investigated here. The closest in properties TMDs are  $2H$ -NbS<sub>2</sub> and NbSe<sub>2</sub>, and both reveal interesting phenomena at low temperatures [44], including CDW and superconductivity. Raman spectra of  $2H$ -NbSe<sub>2</sub> through the transformation to CDW have been extensively studied [44–46]. The Raman spectra demonstrate strongly temperature-dependent excitations (the amplitude modes) and also essentially temperature-independent frozen in modes, the nature of which is often unclear. Several models were proposed to explain the CDW formations. The most common one is Fermi-surface nesting [30], though the importance of Van Hove singularities [47], electronic states

away from the Fermi level [48], Jahn-Teller effect [49], or an excitonic origin [50] was also emphasized. Recently, the momentum-dependent electron-phonon coupling has become the mainstream view [51]. All the assumptions above are based on the electron-phonon coupling which is strong in MoS<sub>2</sub> [52]. The CDW order in MoS<sub>2</sub> is mostly due to the electron-phonon coupling.

The CDW orders in TMDs are classified as weak CDW systems, intermediate CDW systems, and strong CDW systems [53], with different CDW lock-in temperatures ( $T_{\text{CDW}}$ ). Usually speaking, the weak CDW systems are accompanied by a superconductivity state (like  $2H$ -NbSe<sub>2</sub> with  $T_c$  of 7.2 K [8] and  $T_{\text{CDW}}$  of 33.5 K [54]). In intermediate CDW systems,  $T_{\text{CDW}}$  increases from  $2H$ -NbSe<sub>2</sub> (33.5 K), through  $2H$ -TaS<sub>2</sub> (80 K) to  $2H$ -TaSe<sub>2</sub> (122 K). Meanwhile,  $T_c$  decreases from  $2H$ -NbSe<sub>2</sub> (7.2 K) through  $2H$ -TaS<sub>2</sub> (0.8 K) to  $2H$ -TaSe<sub>2</sub> (0.3 K) [38]. The strong CDW compounds ( $1T$ -TiSe<sub>2</sub>,  $1T$ -TaSe<sub>2</sub>, and  $1T$ -TaS<sub>2</sub>) are not even superconductors. However, the superconductivity in  $1T$ -TiSe<sub>2</sub> [55] and  $1T$ -TaS<sub>2</sub> [56] can be induced by pressure, accompanying the suppression of the CDW order. The anomalies in resistance and Raman spectra in MoS<sub>2</sub> reveal that the  $T_{\text{CDW}}$  is about 140 K. Therefore, the CDW order in MoS<sub>2</sub> is between intermediate and strong CDW systems. The superconductivity at higher pressures above 90 GPa [32] can be obtained by restraining the CDW state.

Upon compression above 90 GPa, a superconducting state emerges in MoS<sub>2</sub> below 5 K [32]. CDW and superconductivity in TMDs normally coexist and often are considered to be competing orders. Thus, one can expect a superconducting state to develop in the proximity of a CDW state. The discovery of CDW order in MoS<sub>2</sub> is extremely important since we can classify the superconductivity of MoS<sub>2</sub> as the normal behavior in transition-metal dichalcogenides.

#### IV. CONCLUSIONS

In conclusion, we have reported on electrical transport, and Raman-scattering measurements of MoS<sub>2</sub> at high pressures and low temperatures. The temperature dependencies of the electrical conductivity show anomalies (humps). The Raman spectra also show anomalous behavior in the mixed state revealing a different peak at low temperatures along with the phonon mode softening and broadening. These behaviors suggest the presence of an additional order at low temperature, which creates a modification of the electronic structure (gapping of the Fermi surface) and structural instabilities (CDW). Given a common coexistence and competing of CDW and superconductivity in TMDs, an unusual superconductivity at very high pressures (>80 GPa) is justified.

- [1] K. S. Novoselov, D. Jiang, F. Schedin, T. J. Booth, V. V. Khotkevich, S. V. Morozov, and A. K. Geim, Two-dimensional atomic crystals, *Proc. Natl. Acad. Sci. USA* **102**, 10451 (2005).  
 [2] K. S. Novoselov, A. K. Geim, S. V. Morozov, D. Jiang, M. I. Katsnelson, I. V. Grigorieva, S. V. Dubonos, and A. A. Firsov, Two-dimensional gas of massless Dirac fermions in graphene, *Nature (London)* **438**, 197 (2005).

- [3] B. Radisavljevic, A. Radenovic, J. Brivio, V. Giacometti, and A. Kis, Single-layer MoS<sub>2</sub> transistors, *Nat. Nanotechnol.* **6**, 147 (2011).  
 [4] Q. H. Wang, K. Kalantar-Zadeh, A. Kis, J. N. Coleman, and M. S. Strano, Electronics and optoelectronics of two-dimensional transition metal dichalcogenides, *Nat. Nanotechnol.* **7**, 699 (2012).

- [5] K. I. Bolotin, K. J. Sikes, Z. Jiang, M. Klima, G. Fudenberg, J. Hone, P. Kim, and H. L. Stormer, Ultrahigh electron mobility in suspended graphene, *Solid State Commun.* **146**, 351 (2008).
- [6] K. K. Fung, S. McKernan, J. W. Steed, and J. A. Wilson, Broken hexagonal symmetry in the locked-in state of  $2H_n$ -TaSe<sub>2</sub> and the discommensurate microstructure of its incommensurate CDW states, *J. Phys. C* **14**, 5417 (1981).
- [7] I. Guillaumon, H. Suderow, J. G. Rodrigo, S. Vieira, P. Rodière, L. Cario, E. Navarro-Moratalla, C. Martí-Gastaldo, and E. Coronado, Chiral charge order in the superconductor  $2H$ -TaS<sub>2</sub>, *New J. Phys.* **13**, 103020 (2011).
- [8] E. Revolinsky, G. A. Spiering, and D. J. Beerntsen, Superconductivity in the niobium-selenium system, *J. Phys. Chem. Solid.* **26**, 1029 (1965).
- [9] M. N. Ali, J. Xiong, S. Flynn, J. Tao, Q. D. Gibson, L. M. Schoop, T. Liang, N. Haldolaarachchige, M. Hirschberger, N. P. Ong, and R. J. Cava, Large, non-saturating magnetoresistance in WTe<sub>2</sub>, *Nature (London)* **514**, 205 (2014).
- [10] X. Qian, J. Liu, L. Fu, and J. Li, Quantum spin Hall effect in two-dimensional transition metal dichalcogenides, *Science* **346**, 1344 (2014).
- [11] K. F. Mak, C. Lee, J. Hone, J. Shan, and T. F. Heinz, Atomically Thin MoS<sub>2</sub>: A New Direct-Gap Semiconductor, *Phys. Rev. Lett.* **105**, 136805 (2010).
- [12] K. F. Mak, K. He, J. Shan, and T. F. Heinz, Control of valley polarization in monolayer MoS<sub>2</sub> by optical helicity, *Nat. Nanotechnol.* **7**, 494 (2012).
- [13] H. Zeng, J. Dai, W. Yao, D. Xiao, and X. Cui, Valley polarization in MoS<sub>2</sub> monolayers by optical pumping, *Nat. Nanotechnol.* **7**, 490 (2012).
- [14] D. Xiao, W. Yao, and Q. Niu, Valley-Contrasting Physics in Graphene: Magnetic Moment and Topological Transport, *Phys. Rev. Lett.* **99**, 236809 (2007).
- [15] D. Xiao, G.-B. Liu, W. Feng, X. Xu, and W. Yao, Coupled Spin and Valley Physics in Monolayers of and Other Group-VI Dichalcogenides, *Phys. Rev. Lett.* **108**, 196802 (2012).
- [16] Z. Y. Zhu, Y. C. Cheng, and U. Schwingenschlögl, Giant spin-orbit-induced spin splitting in two-dimensional transition-metal dichalcogenide semiconductors, *Phys. Rev. B* **84**, 153402 (2011).
- [17] H. L. Zhuang, M. D. Johannes, A. K. Singh, and R. G. Hennig, Doping-controlled phase transitions in single-layer, *Phys. Rev. B* **96**, 165305 (2017).
- [18] J. T. Ye, Y. J. Zhang, R. Akashi, M. S. Bahramy, R. Arita, and Y. Iwasa, Superconducting dome in a gate-tuned band insulator, *Science* **338**, 1193 (2012).
- [19] N. F. Q. Yuan, K. F. Mak, and K. T. Law, Possible Topological Superconducting Phases of MoS<sub>2</sub>, *Phys. Rev. Lett.* **113**, 097001 (2014).
- [20] Y. Wang, J. Xiao, H. Zhu, Y. Li, Y. Alsaïd, K. Y. Fong, Y. Zhou, S. Wang, W. Shi, Y. Wang, Z. Alex, E. J. Read, and X. Zhang, Structural phase transition in monolayer MoTe<sub>2</sub> driven by electrostatic doping, *Nature (London)* **550**, 487 (2017).
- [21] Y. Qi, P. G. Naumov, M. N. Ali, C. R. Rajamathi, W. Schnelle, O. Barkalov, M. Hanfland, S.-C. Wu, C. Shekhar, Y. Sun, V. Süß, M. Schmidt, U. Schwarz, E. Pippel, P. Werner, R. Hillebrand, T. Förster, E. Kampert, S. Parkin, R. J. Cava *et al.*, Superconductivity in Weyl semimetal candidate MoTe<sub>2</sub>, *Nat. Commun.* **7**, 11038 (2016).
- [22] Z.-H. Chi, X.-M. Zhao, H. Zhang, A. F. Goncharov, S. S. Lobanov, T. Kagayama, M. Sakata, and X.-J. Chen, Pressure-Induced Metallization of Molybdenum Disulfide, *Phys. Rev. Lett.* **113**, 036802 (2014).
- [23] L. Hromadová, R. Martoňák, and E. Tosatti, Structure change, layer sliding, and metallization in high-pressure MoS<sub>2</sub>, *Phys. Rev. B* **87**, 144105 (2013).
- [24] S. Sugai, K. Murase, S. Uchida, and S. Tanaka, Raman studies of lattice dynamics in  $1T$ -TiSe<sub>2</sub>, *Solid State Commun.* **35**, 433 (1980).
- [25] J. A. Holy, K. C. Woo, M. V. Klein, and F. C. Brown, Raman and infrared studies of superlattice formation in TiSe<sub>2</sub>, *Phys. Rev. B* **16**, 3628 (1977).
- [26] S. Sugai, K. Murase, S. Uchida, and S. Tanaka, Studies of lattice dynamics in  $2H$ -TaS<sub>2</sub> by Raman scattering, *Solid State Commun.* **40**, 399 (1981).
- [27] S. Sugai, Lattice vibrations in the orthorhombic commensurate charge density wave phase of  $2H$ -TaSe<sub>2</sub>, *Solid State Commun.* **44**, 1141 (1982).
- [28] G. K. Scott, K. K. Bardhan, and J. C. Irwin, Raman Scattering from the Orthorhombic Charge-Density-Wave State of  $2H$ -TaSe<sub>2</sub>, *Phys. Rev. Lett.* **50**, 771 (1983).
- [29] T. Wu, H. Mayaffre, S. Krämer, M. Horvatić, C. Berthier, W. N. Hardy, R. Liang, D. A. Bonn, and M.-H. Julien, Magnetic-field-induced charge-stripe order in the high-temperature superconductor YBa<sub>2</sub>Cu<sub>3</sub>O<sub>y</sub>, *Nature (London)* **477**, 191 (2011).
- [30] J. A. Wilson, F. J. Di Salvo, and S. Mahajan, Charge-Density Waves in Metallic, Layered, Transition-Metal Dichalcogenides, *Phys. Rev. Lett.* **32**, 882 (1974).
- [31] A. H. C. Neto, Charge Density Wave, Superconductivity, and Anomalous Metallic Behavior in 2D Transition Metal Dichalcogenides, *Phys. Rev. Lett.* **86**, 4382 (2001).
- [32] Z. Chi, X. Chen, F. Yen, F. Peng, Y. Zhou, J. Zhu, Y. Zhang, X. Liu, C. Lin, S. Chu, Y. Li, J. Zhao, T. Kagayama, Y. Ma, and Z. Yang, Superconductivity in Pristine  $2H_n$ -MoS<sub>2</sub> at Ultrahigh pressure, *Phys. Rev. Lett.* **120**, 037002 (2018).
- [33] L. J. van der Pauw, A method of measuring specific resistivity and Hall effect of discs of arbitrary shape, *Philips Res. Repts.* **13**, 1 (1958).
- [34] A. F. Goncharov, N. Holtgrewe, G. Qian, C. Hu, A. R. Oganov, M. Somayazulu, E. Stavrou, C. J. Pickard, A. Berlie, and F. Yen, Backbone N<sub>x</sub>H compounds at high pressures, *J. Chem. Phys.* **142**, 214308 (2015).
- [35] B. J. Kip and R. J. Meier, Determination of the local temperature at a sample during Raman experiments using Stokes and anti-Stokes Raman bands, *Appl. Spectrosc.* **44**, 707 (1990).
- [36] A. P. Nayak, S. Bhattacharyya, J. Zhu, J. Liu, X. Wu, T. Pandey, C. Jin, A. K. Singh, D. Akinwande, and J.-F. Lin, Pressure-induced semiconducting to metallic transition in multilayered molybdenum disulphide, *Nat. Commun.* **5**, 3731 (2014).
- [37] P. Shen, Q. Li, H. Zhang, R. Liu, B. Liu, X. Yang, Q. Dong, T. Cui, and B. Liu, Raman and IR spectroscopic characterization of molybdenum disulfide under quasi-hydrostatic and non-hydrostatic conditions, *Phys. Status Solidi B* **254**, 1600798 (2017).
- [38] M. Naito and S. Tanaka, Electrical transport properties in  $2H$ -NbS<sub>2</sub>,  $-NbSe_2$ ,  $-TaS_2$  and  $-TaSe_2$ , *J. Phys. Soc. Jpn.* **51**, 219 (1982).

- [39] R. Peierls, *Quantum Theory of Solids* (Oxford University Press, Oxford, 1955).
- [40] J. A. Wilson and A. D. Yoffe, Transition metal dichalcogenides discussion and interpretation of the observed optical, electrical, and structural properties, *Adv. Phys.* **18**, 193 (1969).
- [41] M. V. Klein, Theory of two-phonon Raman scattering in transition metals and compounds, *Phys. Rev. B* **24**, 4208 (1981).
- [42] A. Molina-Sánchez and L. Wirtz, Phonons in single-layer and few-layer MoS<sub>2</sub> and WS<sub>2</sub>, *Phys. Rev. B* **84**, 155413 (2011).
- [43] N. Wakabayashi, H. G. Smith, and R. M. Nicklow, Lattice dynamics of hexagonal MoS<sub>2</sub> studied by neutron scattering, *Phys. Rev. B* **12**, 659 (1975).
- [44] M. A. Méasson, Y. Gallais, M. Cazayous, B. Clair, P. Rodière, L. Cario, and A. Sacuto, Amplitude Higgs mode in the 2H-NbSe<sub>2</sub> superconductor, *Phys. Rev. B* **89**, 060503(R) (2014).
- [45] J. C. Tsang, J. E. Smith, Jr., and M. W. Shafer, Raman Spectroscopy of Soft Modes at the Charge-Density-Wave Phase Transition in 2H-NbSe<sub>2</sub>, *Phys. Rev. Lett.* **37**, 1407 (1976).
- [46] A. Mialitsin, Fano line shape and anti-crossing of Raman active E<sub>2g</sub> peaks in the charge density wave state of NbSe<sub>2</sub>, *J. Phys. Chem. Solids* **72**, 568 (2011).
- [47] T. M. Rice and G. K. Scott, New Mechanism for a Charge-Density-Wave Instability, *Phys. Rev. Lett.* **35**, 120 (1975).
- [48] M. D. Johannes and I. I. Mazin, Fermi surface nesting and the origin of charge density waves in metals, *Phys. Rev. B* **77**, 165135 (2008).
- [49] H. P. Hughes, Structural distortion in TiSe<sub>2</sub> and related materials—a possible Jahn-Teller effect? *J. Phys. C: Solid State Phys.* **10**, L319 (1977).
- [50] H. Cercellier, C. Monney, F. Clerc, C. Battaglia, L. Despont, M. G. Garnier, H. Beck, P. Aebi, L. Patthey, H. Berger, and L. Forró, Evidence for an Excitonic Insulator Phase in 1T-TiSe<sub>2</sub>, *Phys. Rev. Lett.* **99**, 146403 (2007).
- [51] F. Flicker and J. van Wezel, Charge order in NbSe<sub>2</sub>, *Phys. Rev. B* **94**, 235135 (2016).
- [52] H. Li, Q. Zhang, C. C. R. Yap, B. K. Tay, T. H. T. Edwin, A. Olivier, and D. Baillargeat, From bulk to monolayer MoS<sub>2</sub> : Evolution of Raman scattering, *Adv. Funct. Mater.* **22**, 1385 (2012).
- [53] N. Nagaosa and E. Hanamura, Microscopic theory of Raman and infrared spectra of transition-metal dichalcogenides in the charge-density-wave state, *Phys. Rev. B* **29**, 2060 (1984).
- [54] D. E. Moncton, J. D. Axe, and F. J. Disalvo, Study of Superlattice Formation in 2H-NbSe<sub>2</sub> and 2H-TaSe<sub>2</sub> by Neutron Scattering, *Phys. Rev. Lett.* **34**, 734 (1975).
- [55] A. F. Kusmartseva, B. Sipoš, H. Berger, L. Forró, and E. Tutiš, Pressure Induced Superconductivity in Pristine 1T-TiSe<sub>2</sub>, *Phys. Rev. Lett.* **103**, 236401 (2009).
- [56] B. Sipoš, A. F. Kusmartseva, A. Akrap, H. Berger, L. Forró, and E. Tutiš, From Mott state to superconductivity in 1T-TaS<sub>2</sub>, *Nat. Mater.* **7**, 960 (2008).